Research Article | Vol. 8, No. 7 | 1 Jul 2017 | BIOMEDICAL OPTICS EXPRESS 3329
Biomedical Optics EXPRESS

Chip-on-the-tip compact flexible endoscopic epifluorescence video-microscope for in-vivo imaging in medicine and biomedical research

GREGOR MATZ,[1,2] BERNHARD MESSERSCHMIDT,[1,*] WERNER GÖBEL,[3] SEVERIN FILSER,[4] CHRISTIAN S. BETZ,[5] MATTHIAS KIRSCH,[6] ORTRUD UCKERMANN,[6] MARCEL KUNZE,[1] SVEN FLÄMIG,[1] ANDRÉ EHRHARDT,[3] KLAUS-MARTIN IRION,[3] MAREIKE HAACK,[5] MARIO M. DOROSTKAR,[4] JOCHEN HERMS,[4] AND HERBERT GROSS,[2]

[1] *GRINTECH GmbH, Schillerstrasse 1, 07743 Jena, Germany*
[2] *Institute of Applied Physics, FSU Jena, Fürstengraben 1, 07737 Jena, Germany*
[3] *KARL STORZ GmbH & Co. KG, Mittelstrasse 8, 78532 Tuttlingen, Germany*
[4] *LMU Munich, Geschwister-Scholl-Platz 1, 80539 Munich, Germany*
[5] *Klinikum Großhadern, Marchioninistr. 13, 81377 Munich, Germany*
[6] *Neurosurgery, University Hospital Carl Gustav Carus, TU Dresden, Fetscherstrasse 74, 01307 Dresden, Germany*
[*] *messerschmidt@grintech.de*

Abstract: We demonstrate a 60 mg light video-endomicroscope with a cylindrical shape of the rigid tip of only 1.6 mm diameter and 6.7 mm length. A novel implementation method of the illumination unit in the endomicroscope is presented. It allows for the illumination of the biological sample with fiber-coupled LED light at 455 nm and the imaging of the red-shifted fluorescence light above 500 nm in epi-direction. A large numerical aperture of 0.7 leads to a sub-cellular resolution and yields to high-contrast images within a field of view of 160 μm. A miniaturized chip-on-the-tip CMOS image sensor with more than 150,000 pixels captures the multicolor images at 30 fps. Considering size, plug-and-play capability, optical performance, flexibility and weight, we hence present a probe which sets a new benchmark in the field of epifluorescence endomicroscopes. Several ex-vivo and in-vivo experiments in rodents and humans suggest future application in biomedical fields, especially in the neuroscience community, as well as in medical applications targeting optical biopsies or the detection of cellular anomalies.

OCIS codes: (170.2150) Endoscopic imaging; (350.3950) Micro-optics; (170.3880) Medical and biological imaging; (170.3890) Medical optics instrumentation; (180.2520) Fluorescence microscopy.

References and links

1. B. A. Flusberg, J. C. Jung, E. D. Cocker, E. P. Anderson, and M. J. Schnitzer, "In vivo brain imaging using a portable 3.9 gram two-photon fluorescence microendoscope," Opt. Lett. **30**, 2272–2274 (2005).
2. D. R. Rivera, C. M. Brown, D. G. Ouzounov, I. Pavlova, D. Kobat, W. W. Webb, and C. Xu, "Compact and flexible raster scanning multiphoton endoscope capable of imaging unstained tissue," Proc. Natl. Acad. Sci. **108**, 17598–17603 (2011).
3. J. Sawinski, D. J. Wallace, D. S. Greenberg, S. Grossmann, W. Denk, and J. N. Kerr, "Visually evoked activity in cortical cells imaged in freely moving animals," Proc. Natl. Acad. Sci. **106**, 19557–19562 (2009).
4. F. Helmchen, M. S. Fee, D. W. Tank, and W. Denk, "A miniature head-mounted two-photon microscope: high-resolution brain imaging in freely moving animals," Neuron **31**, 903–912 (2001).
5. K. K. Ghosh, L. D. Burns, E. D. Cocker, A. Nimmerjahn, Y. Ziv, A. El Gamal, and M. J. Schnitzer, "Miniaturized integration of a fluorescence microscope," Nat. methods **8**, 871–878 (2011).
6. J. C. Jung, A. D. Mehta, E. Aksay, R. Stepnoski, and M. J. Schnitzer, "In vivo mammalian brain imaging using one-and two-photon fluorescence microendoscopy," J. Neurophysiol. **92**, 3121–3133 (2004).
7. R. P. Barretto, B. Messerschmidt, and M. J. Schnitzer, "In vivo fluorescence imaging with high-resolution microlenses," Nat. methods **6**, 511–512 (2009).

#288032 https://doi.org/10.1364/BOE.8.003329
Journal © 2017 Received 3 Apr 2017; revised 15 Jun 2017; accepted 15 Jun 2017; published 20 Jun 2017

Biomedical Optics EXPRESS

8. M. Osanai, T. Suzuki, A. Tamura, T. Yonemura, I. Mori, Y. Yanagawa, H. Yawo, and H. Mushiake, "Development of a micro-imaging probe for functional brain imaging," Neurosci. Res. **75**, 46–52 (2013).
9. M. E. Bocarsly, W.-C. Jiang, C. Wang, J. T. Dudman, N. Ji, and Y. Aponte, "Minimally invasive microendoscopy system for in vivo functional imaging of deep nuclei in the mouse brain," Biomed. Opt. Express **6**, 4546–4556 (2015).
10. E. Segev, J. Reimer, L. C. Moreaux, T. M. Fowler, D. Chi, W. D. Sacher, M. Lo, K. Deisseroth, A. S. Tolias, A. Faraon, and M. L. Roukes, "Patterned photostimulation via visible-wavelength photonic probes for deep brain optogenetics," Neurophotonics **4**, 011002 (2017).
11. R. P. Barretto, T. H. Ko, J. C. Jung, T. J. Wang, G. Capps, A. C. Waters, Y. Ziv, A. Attardo, L. Recht, and M. J. Schnitzer, "Time-lapse imaging of disease progression in deep brain areas using fluorescence microendoscopy," Nat. med. **17**, 223–228 (2011).
12. M. E. Llewellyn, R. P. Barretto, S. L. Delp, and M. J. Schnitzer, "Minimally invasive high-speed imaging of sarcomere contractile dynamics in mice and humans," Nature **454**, 784–788 (2008).
13. J. Hung, S. Lam, J. C. Leriche, and B. Palcic, "Autofluorescence of normal and malignant bronchial tissue," Lasers Surg. Med. **11**, 99–105 (1991).
14. D. Frimberger, D. Zaak, H. Stepp, R. Knüchel, R. Baumgartner, P. Schneede, N. Schmeller, and A. Hofstetter, "Autofluorescence imaging to optimize 5-ALA-induced fluorescence endoscopy of bladder carcinoma," Urology **58**, 372–375 (2001).
15. Z. Huang,W. Zheng, S. Xie, R. Chen, H. Zeng, D. I. McLean, and H. Lui, "Laser-induced autofluorescence microscopy of normal and tumor human colonic tissue," Int. J. Oncol. **24**, 59–64 (2004).
16. L. Thiberville, S. Moreno-Swirc, T. Vercauteren, E. Peltier, C. Cavé, and G. Bourg Heckly, "In vivo imaging of the bronchial wall microstructure using fibered confocal fluorescence microscopy," Am. J. Respir. Crit. Care Med. **175**, 22–31 (2007).
17. C. Betz, M. Mehlmann, K. Rick, H. Stepp, G. Grevers, R. Baumgartner, and A. Leunig, "Autofluorescence imaging and spectroscopy of normal and malignant mucosa in patients with head and neck cancer," Lasers Surg. Med. **25**, 323–334 (1999).
18. A. L. Polglase, W. J. McLaren, S. A. Skinner, R. Kiesslich, M. F. Neurath, and P. M. Delaney, "A fluorescence confocal endomicroscope for in vivo microscopy of the upper-and the lower-GI tract," Gastrointest. endosc. **62**, 686–695 (2005).
19. P.-L. Hsiung, J. Hardy, S. Friedland, R. Soetikno, C. B. Du, A. P. Wu, P. Sahbaie, J. M. Crawford, A. W. Lowe, C. H. Contag et al., "Detection of colonic dysplasia in vivo using a targeted heptapeptide and confocal microendoscopy," Nat. med. **14**, 454–458 (2008).
20. C. M. Lee, C. J. Engelbrecht, T. D. Soper, F. Helmchen, and E. J. Seibel, "Scanning fiber endoscopy with highly flexible, 1-mm catheterscopes for wide-field, full-color imaging," J. Biophotonics **3**, 385 (2010).
21. D. A. Dombeck, A. N. Khabbaz, F. Collman, T. L. Adelman, and D. W. Tank, "Imaging large-scale neural activity with cellular resolution in awake, mobile mice," Neuron **56**, 43–57 (2007).
22. A. Holtmaat, T. Bonhoeffer, D. K. Chow, J. Chuckowree, V. De Paola, S. B. Hofer, M. Hübener, T. Keck, G. Knott,W.-C. A. Lee et al., "Long-term, high-resolution imaging in the mouse neocortex through a chronic cranial window," Nat. Protoc. **4**, 1128–1144 (2009).
23. H. Dana, T.-W. Chen, A. Hu, B. C. Shields, C. Guo, L. L. Looger, D. S. Kim, and K. Svoboda, "Thy1-GCaMP6 transgenic mice for neuronal population imaging in vivo," PLoS One **9**, e108697 (2014).
24. A. Miyawaki, O. Griesbeck, R. Heim, and R. Y. Tsien, "Dynamic and quantitative Ca^{2+} measurements using improved cameleons," Proc. Natl. Acad. Sci. **96**, 2135–2140 (1999).
25. J. M. Gee, M. B. Gibbons, M. Taheri, S. Palumbos, S. C. Morris, R. M. Smeal, K. F. Flynn, M. N. Economo, C. G. Cizek, M. R. Capecchi et al., "Imaging activity in astrocytes and neurons with genetically encoded calcium indicators following in utero electroporation," Front. Mol. Neurosci. **8**, 425 (2015).
26. C. Stosiek, O. Garaschuk, K. Holthoff, and A. Konnerth, "In vivo two-photon calcium imaging of neuronal networks," Proc. Natl. Acad. Sci. **100**, 7319–7324 (2003).
27. K. Ohki, S. Chung, Y. H. Ch'ng, P. Kara, and R. C. Reid, "Functional imaging with cellular resolution reveals precise micro-architecture in visual cortex," Nature **433**, 597–603 (2005).
28. S. R. Schultz, K. Kitamura, A. Post-Uiterweer, J. Krupic, and M. Häusser, "Spatial pattern coding of sensory information by climbing fiber-evoked calcium signals in networks of neighboring cerebellar purkinje cells," J. Neurosci. **29**, 8005–8015 (2009).
29. B. Lendvai, E. A. Stern, B. Chen, and K. Svoboda, "Experience-dependent plasticity of dendritic spines in the developing rat barrel cortex in vivo," Nature **404**, 876–881 (2000).
30. R. M. Hoffman, "Green fluorescent protein imaging of tumour growth, metastasis, and angiogenesis in mouse models," Lancet Oncol. **3**, 546–556 (2002).
31. H.-U. Dodt, U. Leischner, A. Schierloh, N. Jährling, C. P. Mauch, K. Deininger, J. M. Deussing, M. Eder, W. Zieglgänsberger, and K. Becker, "Ultramicroscopy: three-dimensional visualization of neuronal networks in the whole mouse brain," Nat. methods **4**, 331–336 (2007).
32. C. Laperchia, A. L. A. Mascaro, L. Sacconi, A. Andrioli, A. Matté, L. De Franceschi, G. Grassi-Zucconi, M. Bentivoglio, M. Buffelli, and F. S. Pavone, "Two-photon microscopy imaging of Thy1 GFP-m transgenic mice: A novel animal model to investigate brain dendritic cell subsets in vivo," PloS one **8**, e56144 (2013).
33. F. M. Bareyre, M. Kerschensteiner, T. Misgeld, and J. R. Sanes, "Transgenic labeling of the corticospinal tract for

Biomedical Optics EXPRESS

monitoring axonal responses to spinal cord injury," Nat. med. **11**, 1355–1360 (2005).
34. K. Bulloch, M. M. Miller, J. Gal-Toth, T. A. Milner, A. Gottfried-Blackmore, E. M.Waters, U.W. Kaunzner, K. Liu, R. Lindquist, M. C. Nussenzweig, "CD11c/EYFP transgene illuminates a discrete network of dendritic cells within the embryonic, neonatal, adult, and injured mouse brain," J. Comp. Neurol. **508**, 687–710 (2008).
35. R. Christie, B. Bacskai, W. Zipfel, R. Williams, S. Kajdasz, W. Webb, and B. Hyman, "Growth arrest of individual senile plaques in a model of alzheimer's disease observed by in vivo multiphoton microscopy," J. Neurosci. **21**, 858–864 (2001).
36. O. Uckermann, R. Galli, S. Leupold, R. Coras, M. Meinhardt, S. Hallmeyer-Elgner, T. Mayer, A. Storch, G. Schackert, E. Koch et al., "Label-free multiphoton microscopy reveals altered tissue architecture in hippocampal sclerosis," Epilepsia **58** (2017).
37. G. A. Sonn, S.-N. E. Jones, T. V. Tarin, C. B. Du, K. E. Mach, K. C. Jensen, and J. C. Liao, "Optical biopsy of human bladder neoplasia with in vivo confocal laser endomicroscopy," J. Urology **182**, 1299–1305 (2009).
38. Z. Huang, S. Shi, H. Qiu, D. Li, J. Zou, and S. Hu, "Fluorescence-guided resection of brain tumor: review of the significance of intraoperative quantification of protoporphyrin IX fluorescence," Neurophotonics **4**, 011011 (2017).
39. C. J. Engelbrecht, R. S. Johnston, E. J. Seibel, and F. Helmchen, "Ultra-compact fiber-optic two-photon microscope for functional fluorescence imaging in vivo," Opt. Express **16**, 5556–5564 (2008).
40. W. Göbel, J. N. Kerr, A. Nimmerjahn, and F. Helmchen, "Miniaturized two-photon microscope based on a flexible coherent fiber bundle and a gradient-index lens objective," Opt. Lett. **29**, 2521–2523 (2004).
41. S. M. Landau, C. Liang, R. T. Kester, T. S. Tkaczyk, and M. R. Descour, "Design and evaluation of an ultra-slim objective for in-vivo deep optical biopsy," Opt. Express **18**, 4758–4775 (2010).
42. A. Lukic, S. Dochow, H. Bae, G. Matz, I. Latka, B. Messerschmidt, M. Schmitt, and J. Popp, "Endoscopic fiber probe for nonlinear spectroscopic imaging," Optica **4**, 496–501 (2017).
43. E. Laemmel, M. Genet, G. Le Goualher, A. Perchant, J.-F. Le Gargasson, and E. Vicaut, "Fibered confocal fluorescence microscopy (cell-vizio^{TM}) facilitates extended imaging in the field of microcirculation," J. Vasc. Res. **41**, 400–411 (2004).
44. G. Matz, B. Messerschmidt, and H. Gross, "Design and evaluation of new color-corrected rigid endomicroscopic high NA grin-objectives with a sub-micron resolution and large field of view," Opt. Express **24**, 10987–11001 (2016).
45. A. C. Kwan, K. Duff, G. K. Gouras, and W. W. Webb, "Optical visualization of Alzheimer's pathology via multiphoton-excited intrinsic fluorescence and second harmonic generation," Opt. Express **17**, 3679–3689 (2009).
46. A. N. Siakotos, I. Watanabe, A. Saito, and S. Fleischer, "Procedures for the isolation of two distinct lipopigments from human brain: lipofuscin and ceroid," Biochem. Med. **4**, 361–375 (1970).
47. S. M. Arribas, C. J. Daly, M. C. Gonzáles, and J. C. McGrath, "Imaging the vascular wall using confocal microscopy," J. Physiol. **584**, 5–9 (2007).
48. D. Yin, "Biochemical basis of lipofuscin, ceroid, and age pigment-like fluorophores," Free Radic. Biol. Med. **21**, 871–888 (1996).
49. C. Laperchia, A. L. A. Mascaro, L. Sacconi, A. Andrioli, A. Mattè, L. D. Franceschi, G. Grassi-Zucconi, M. Bentivoglio, M. Buffelli, and F. S. Pavone, "Two-photon microscopy imaging of thy1 GFP-M transgenic mice: A novel animal model to investigate brain dendritic cell subsets in vivo," PloS one **8**, e56144 (2013).
50. F. Yuan, H. A. Salehi, Y. Boucher, U. S. Vasthare, R. F. Tuma, and R. K. Jain, "Vascular permeability and microcirculation of gliomas and mammary carcinomas transplanted in rat and mouse cranial windows," Cancer Res. **54**, 4564–4568 (1994).
51. A. Holtmaat, T. Bonhoeffer, D. K. Chow, J. Chuckowree, V. De Paola, S. B. Hofer, M. Hübener, T. Keck, G. Knott,W.-C. A. Lee, "Long-term, high-resolution imaging in the mouse neocortex through a chronic cranial window," Nat. Protoc. **4**, 1128–1144 (2009).

1. Introduction

Using fluorescence endoscopy to visualize regions inside a living organism which are too deep to reach with traditional, table-top microscopes has drawn great interest in recent years, especially in biomedical research [1–11] and medical fields [12–20]. In biology, attention originates from the neuroscience community which aims to achieve deeper insights of how the brain works by correlating cellular activity in neuronal subpopulations with animal behavior [21–23]. In this context, tiny and highly flexible devices are required which can be attached to the head of the animal to image behaviorally evoked brain zone activities over long time periods [3–5]. Fluorescence imaging modalities proved to be especially useful in this scope of application due to their ability to observe neuronal spikings in real time after a viral transduction of genetically encoded calcium indicators [23–25] or synthetic dyes [26–28], and represent the method of choice for respective endomicroscopes. Moreover, the modality allows for long-term observations of a sparse subset of neuronal populations in genetically modified mice expressing enhanced

Biomedical Optics EXPRESS

green [29–31,49] or yellow [33,34] fluorescent proteins. Further biomedical applications are rather closely related to medical aims and seek for a profound understanding of how the progression of diseases correlate with morphological changes on the cellular level [11,12,35,36] to prospectively draw conclusions on possible cures. Furthermore, fluorescence modalities bear large potentials in medical fields for a delineation of healthy from precancerous or cancerous lesions during surgical interventions in real time by taking optical biopsies. A reliable distinction comparable to established pathologist methods can thus be achieved by a spectrally and spatially resolved evaluation of the autofluorescence signals [13–16] or by similar analyses using medically-licensed fluorescent dyes [18,37,38].

Two different fluorescence imaging modalities are applied in todays endomicroscopes, namely single- and multi-photon processes. Multi-photon fluorescence microscopy allows for inherent optical sectioning but requires expensive pico- or femto-second pulsed lasers and a bulky scanning mechanism incorporated in the head of the probe [1–4, 39]. Approaches have been established, which externalize the scanning unit by utilizing a multicore fiber [40–42] and therewith tremendously miniaturized the size of the rigid tip. Yet, a finite bending radius of the flexible part comes along with a complex and costly coupling setup at the proximal side of the fiber probe and hence impede the transfer into the daily healthcare practice and research community.

On the other hand, flexible probes based on single-photon epi-fluorescence imaging modalities are highly promising but still suffer from different drawbacks. State-of-the-art fiber scanning endoscopic devices achieve tiny outer diameters of 1.0 mm but come along with a complex and fragile scanning mechanism as well as the necessity of frequent recalibrations [20]. Fiber bundle approaches are limited in respect of the bending radius, incorporate expensive fibers and suffer from a low resolution [43]. Other devices achieve high robustness, affordable prices and reliable plug-and-play mechanisms by using chip-on-the-tip image sensors, however with a limited minimal size of 2.4 cm^3 and a weight of 1.9 g [5]. Further approaches achieve very tiny diameters and an easy implementation but only a low image quality [8].

Here, we present a highly flexible endoscopic probe which is based on epi-fluorescence imaging modalities and compensates for appearing weaknesses of state-of-the-art-systems. Thus, the probe convinces due to a reduced size of the rigid tip of only 6.7 mm length and 1.6 mm diameter, a low weight of 60 mg, a high robustness and flexibility, an improved optical performance comparable to what is achieved by commercially available table-top microscopes as well as an easy plug-and-play usability.

2. Results

2.1. Optical design and mechanical setup

In this publication, we present a novel approach of an epi-fluorescence illumination realized by combining a side-fire fiber and a dichroic beam splitter as sketched in Fig. 1. For this purpose, we fixed a 180 μm small microprism at the distal end of a multimode fiber (NA 0.22±0.02, core diameter 100±2 μm) and thus realize a 90 degree deflection of the subassembly. Moreover, we utilized fiber-coupled light with a peak emission wavelength of 455 nm and a spectral bandwidth at 50 % maximum intensity of 25 nm which enables sufficient excitation of a broad range of markers (e.g. eGFP, GCaMP6 and Fluorescein) as well as endogenous fluorophores. As indicated in the drawing, a 500 nm long-pass filter located in the pupil of the imaging ray paths realizes a second deflection by 90 degree and a following multi-lens objective enables a homogeneous illumination of the specimen. For a good scratch and crack resistance, the objective is covered with a sapphire window and assures an additional working distance through a 170 μm thick N-BK7 coverslip plus 60 μm in tissue. Photons emitted from the sample are hence collected by the same multilens objective within a quadratic field of view of 173 μm side length with a

Biomedical Optics EXPRESS

numerical aperture of 0.7. The red shifted fluorescence light with wavelengths above 500 nm can hence pass the longpass filter located in the pupil. Finally, the resolving image which represents the observed object magnified by a factor of 4.1 is captured by a compact CMOS RGB image sensor with a resolution of more than 150,000 pixels and a frame rate of 30 fps. The customized quadratic CMOS camera packaging, electronics and software was developed and provided by KARL STORZ GmbH & Co. KG. The multilens objective combines gradient index lenses and tiny spherical microcomponents to achieve the high numerical aperture and simultaneously promise a homogeneous resolution within the entire field of view. All spherical microlenses and GRIN-lenses of 1.0 mm in diameter incorporated in probe were designed according to the concepts in [44], adapted to the beam splitting approach shown in Fig. 1 and manufactured in collaboration between KARL STORZ GmbH & Co. KG and GRINTECH GmbH.

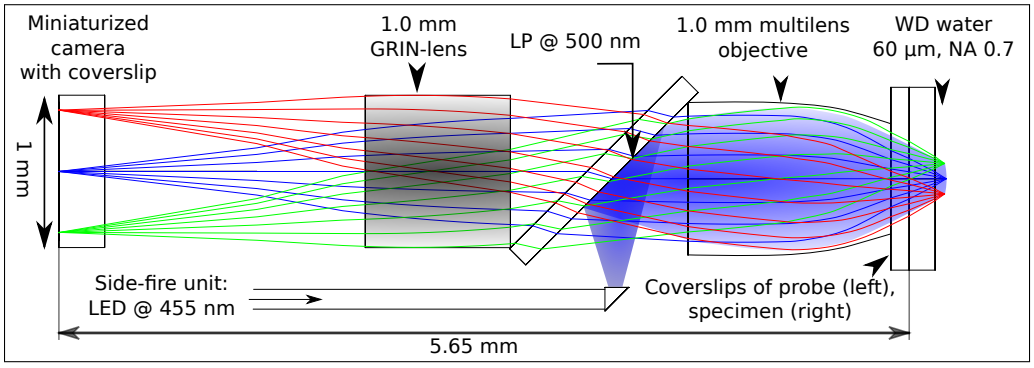

Fig. 1. Optical design of the endoscopic probe based on a double deflection approach using a side-fire fiber and a 500 nm longpass filter. Peak emission of the incoherent illumination light source (LED) at 455 nm and imaging of the red shifted fluorescence light on a subcellular level with a numerical aperture of 0.7. Object is magnified by a factor of 4.1 and captured by a miniaturized CMOS image sensor chip with more than 150,000 pixels.

Previous experiments pointed out that a broad spectral range and reduced coherence length of the illumination light source is required to prevent speckle pattern and mode structures. Light emitting diodes (LED) combine those advantages and show hence a large potential for uniform illumination concepts. However, the significant mismatch of the Etendue between the LED and the utilized multimode fiber comes along with a strictly confined coupling efficiency and hence a low illumination power at the specimen. A custom 1.8 mm GRIN lens was used to optimize the coupling efficiency between the LED and the step index fiber due to the necessary working distance in front of the LED chip. A coupling efficiency of less than 1 % in the 100 μm fiber compared to the total emitted LED power was achieved. Yet, the precise overlap of the illuminated tissue region and the imaged part as well as a high photon collection efficiency realized by a large object-side numerical aperture are unique features of the presented approach and enable the imaging capability in real time with minimal illumination power measured at the distal tip of less than 60 μW spread homogeneously within the observed region.

After that, we evaluated the optical imaging performance by ray tracing algorithms with the commercially available software ZEMAX (ZEMAX 13 Release 2 SP1 Professional, Radiant, Redmont, WA). At first, we evaluated the axial shift of the image plane at the center of the field of view per nm wavelength displacement. At the current state of development we obtained a linearly approximated value of 0.15 μm per nm progressively decreasing for increasing wavelengths. Considering the limited spectral range of typical fluorophores and to minimize complexity and cost of the probe, we abstained from incorporating a color correction which would have added one more doublet lens or diffractive optical element [44]. Subsequently, we selected the

Biomedical Optics EXPRESS

monochromatic Strehl ratio (@532 nm) as a meaningful design criterion to analyze the imaging performance of the system and depicted its magnitude in Fig. 2(a) depending on the field point position. We can denote the optical performance to be diffraction limited within the entire field of view according to a Strehl ratio larger than 0.8. Due to the camera chip size and the corresponding magnification of the optical setup we limited the evaluation area to a quadratic field size with a side length of 173 μm. Secondly, we replaced the latter mentioned field with a Siemens-star-type object as drawn in Fig. 2(b) (left) and simulated the image monochromatically with standard ray-trace algorithms at a wavelength of 532 nm. The result is depicted in Fig. 2(b) (right) and reveals qualitatively an excellent point-to-point imaging performance of the optical assembly. However, minor pincushion distortion effects up to 2.5 % incrementally emerge for progressively increasing field zone diameters as seen in the simulated image which however can be numerically corrected once qualified precisely. Furthermore, an object sided field curvature of 6 μm between the optical axis and the margin of the field of view remains in the design. Yet, a limited amount of distortion and field curvature is tolerable in medical and biological applications due to the observation of volume tissue and the rather phenomenological than spatially accurate demand on the images.

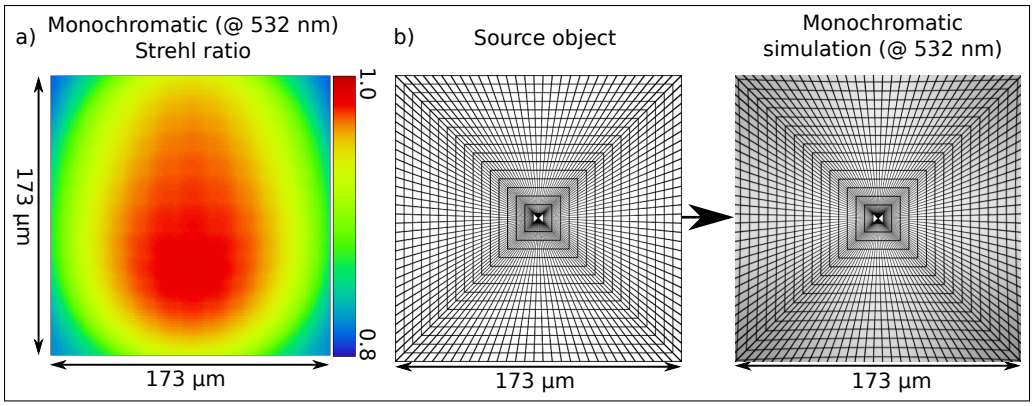

Fig. 2. a) Monochromatic (@ 532 nm) Strehl ratio indicates a diffraction limited performance (Strehl ratio≥0.8) within the entire field of view. Consideration of a quadratic object with 173 μm side length. b) Monochromatic image simulation (@ 532 nm) of a Siemens-star-type object (left) observed through the endomicroscope (right) confirms the excellent point-to-point image quality but exposes slight vignetting and pincushion distortion effects progressively increasing towards the edge of the field of view. The pixelation of the camera chip is not considered. Scale in object space (Evaluations performed with ZEMAX).

Figure 3(a) depicts the oval-shape dichroic beam splitter fixed inside the final mechanical mounting. The right side of the same figure illustrates the small appearance of the rigid tip of the endoscope next to a matchstick and demonstrates the miniaturized extent of the cylindrical device of 6.7 mm length and 1.6 mm diameter with a weight of only 60±10 mg excluding the wires. Not illustrated in total length are the two 1.0 meter long wires which are attached to the backside of the probe head. The thin wire seen in the figure corresponds to the multimode fiber and guides the illumination light towards the rigid tip of the device whereas the second one controls the camera unit and is connected to an image processing unit provided by KARL STORZ GmbH & Co. KG. This unit represents the interface of the device and enables the user by plug-and-play characteristics to visualize and possibly store the real-time RGB images with 30 frames per second.

Biomedical Optics EXPRESS

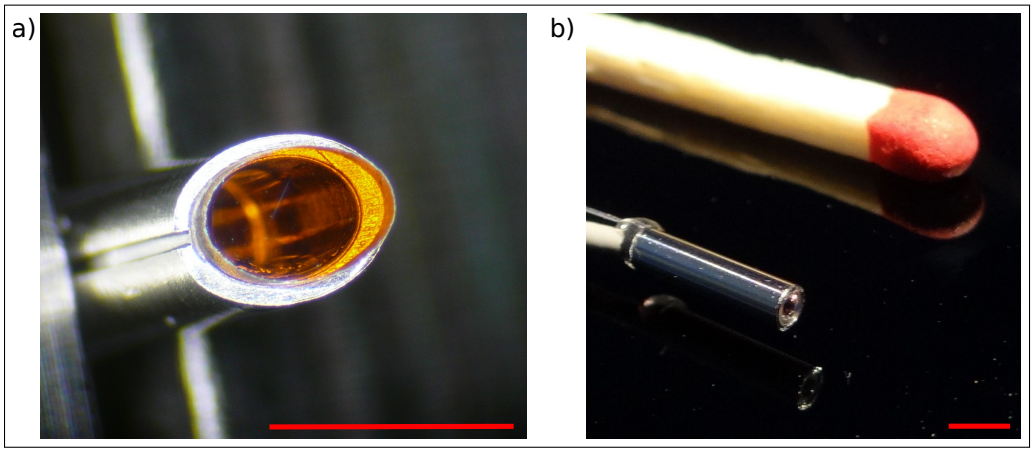

Fig. 3. a) Oval-shape 500 nm long-pass dichroic beam splitter fixed inside the final mechanical mounting. b) Size comparison of a customary matchstick next to the final probe illustrates the miniature appearance of the device with a spatial extent of only 1.6 mm in diameter, a length of 6.7 mm and a total weight of 60±10 mg excluding the wires. Scale bars 2.0 mm, respectively.

2.2. Resolution experiments

For a first proof of principle, a chrome grid with a line width and spacing between consecutive structures of 16 μm respectively has been placed on top of a homogeneously fluorescent target, covered with a 170 μm thick N-BK7 coverslip, immersed in water from both sides and finally imaged with the endomicroscopic probe. Therefore, the objective has been attached to a five axis stage and axially adjusted so that the on-axis position became sharply focused while illuminating the sample homogeneously in epi-direction at 455 nm. Qualitatively, an optimal imaging performance has been achieved at the highest possible intensity of 55±5 μW which has thus been utilized for all proceeding experiments. This has been possible since the camera regulated the integration time automatically and thus prevented an overexposure when imaging strongly fluorescent specimens. Figure 4(a) depicts the image captured with the presented probe and indicates a homogeneously high resolving image performance within the entire field of view.

Furthermore, two slight aberrations influence the optical performance in the corners of the image. These include a minor pincushion distortion effect comparable to what has been simulated in Fig. 2(b)(right). Moreover, a slightly degrading optical performance is observed when progressively approaching the edge of the field of view which results from the incipient field curvature of the probe. A reduction of the distance between the objective and the cover glass by 5±2 μm came along with a sharpening of the corners while slightly blurring the center of the field of view simultaneously (results not shown). Furthermore, the measurement extracts a length and height of the field of view of 164±2 μm which shows a minor discrepancy to the design value discussed in chapter 2.1 of about -5 %. A possible explanation of the observed mismatch is given by a slight axial misalignment of the camera. Simulations with ZEMAX confirmed that such a misalignment can lead to the observed difference in magnification without a significant reduction in resolution. Prospectively, a more precise alignment of the camera unit in future assemblies can circumvent the observed difference.

Figure 4(b) depicts the radial intensity profile obtained by integrating the pixels within the red rectangle shown in Fig. 4(a) along the y-axis and plotting the normalized value in dependency of the x-axis position. The large background seen in the graph results most likely from multiple reflections between the high refractive index sapphire cover window of the probe and the highly

Biomedical Optics EXPRESS

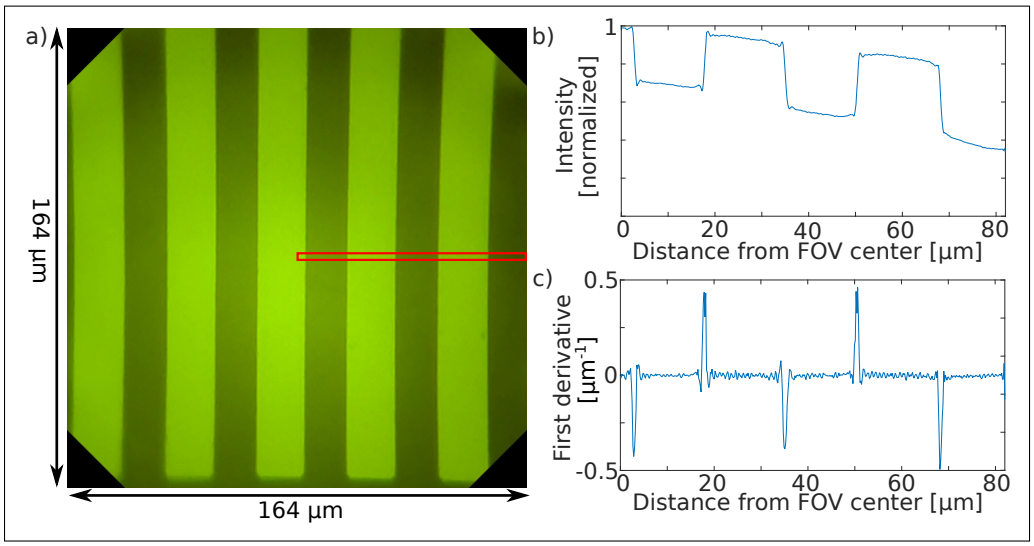

Fig. 4. a) Image captured with the endomicroscopic probe of a uniform chrome grid with a period of 32 μm placed in front of a homogeneously fluorescent target illuminated in epi-direction. A highly resolving image quality is obtained. Slight pincushion distortion effects are visible and progressively increase towards the edge of the field of view. b) Radial intensity profile obtained within the red rectangle in (a) indicates precise edge response functions as a function of the radial distance from the optical axis. c) The first derivative of the edge response function (b) shows the line spread function. Its full-width-at-half-maximum is a measure for the resolution of the device. Averaged FWHM of 0.74±0.08 μm has been obtained.

reflecting grid and is not inherent to the optical assembly. The steepness of the obtained edge response functions at different radial positions hence correlate with the spatial resolution at the corresponding field zone. To quantitatively obtain a measure for the resolution we thus calculated the first derivative of the edge response functions numerically with MATLAB (R2015a, The MathWorks, Natick, MA) and thus obtained the line spread functions depicted in Fig. 4(c). The full-width-at-half-maximum (FWHM) of the corresponding five peaks led to a mean value of 0.74±0.08 μm, which correlates to the pixelation of the image sensor (0.42 μm in object space). Additional experimentally obtained results of equivalent setups confirmed that the specified standard deviation of 0.08 μm results from the uncertainty of the measurement and is neither inherent to the assembly nor to the imaged field zone position which affirms the homogeneous resolution within the entire field of view. Due to the discretization of the camera we couldn't however obtain the theoretically achievable resolution given by the Abbe-limit and thus showed, that the camera chip rather than the optical components limit the resolution. Hence, future developments within the camera chip industry might further improve the resolution of the presented endomicroscope.

2.3. *In-vitro applications*

Subsequently, a fresh leaf of *Begonia x ricinifolia* has been soaked with water, positioned on a glass wafer and covered with a 170 μm thick N-BK7 coverslip. By analogy with the previous experiment, the endoscopic probe has been attached to a five axis stage and positioned on top of the coverslip to enable for the adjustment of the axial focus position by mechanically moving the probe in the axial direction. Furthermore, a small drop of water prevented an air gap between the

Biomedical Optics EXPRESS

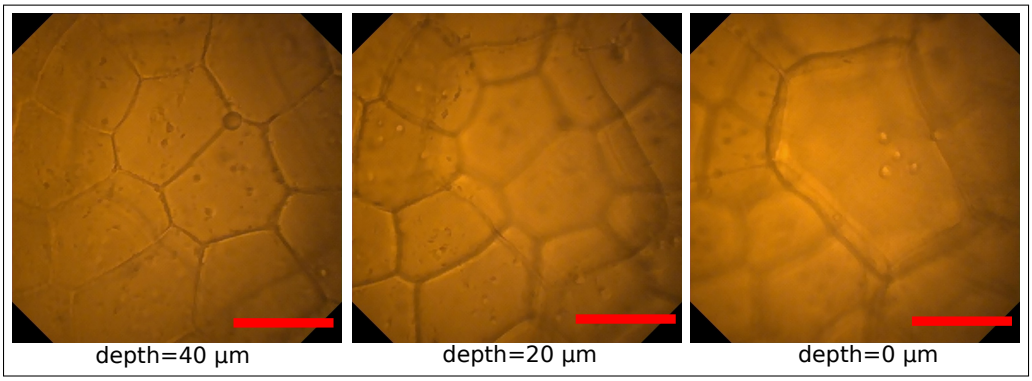

Fig. 5. Pictures of the upper surface of a leaf of *Begonia x ricinifolia* captured with the endomicroscope at the same lateral position but at different axial distances. Probe has been attached to a five-axis stage and moved mechanically away from the specimen in 20 μm steps (from left to right). The ability to sharply image the different axial tissue layers consisting of different cell sizes with a uniformly high resolution but slight intensity reduction for deeper layers is observed. Scale bars 50 μm, respectively.

probe and the sample and hence avoided undesired spherical aberrations. Figure 5 depicts images of the leaf at the same lateral position but at different axial distances between the probe and the specimen which increase by 20 μm (from left to right) respectively and demonstrate impressively the ability of the probe to clearly distinguish and sharply image at different axial depths without confocal imaging approaches. Due to the dominating red fluorescence behavior the leaf tissue appears in red.

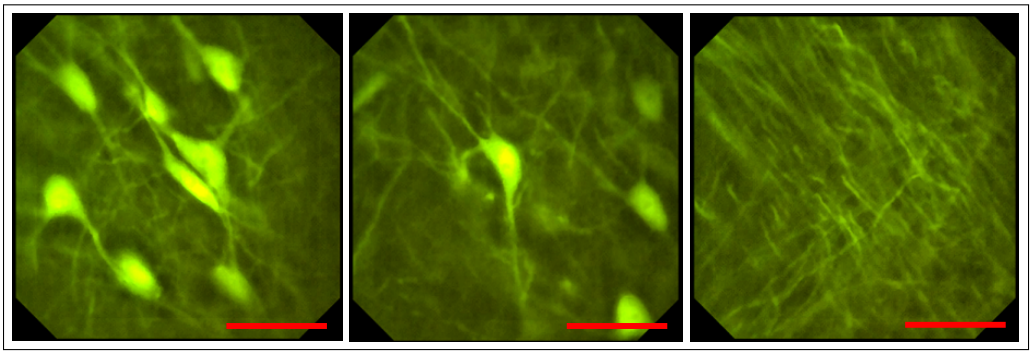

Fig. 6. Pictures captured with the endomicroscopic probe of a thin histological brain slice of a transgenic Thy1-GFP-M mouse expressing enhanced green fluorescent protein in a sparse subset of neuronal populations. Illumination in epi-direction. The submicrometer resolution enables the visualization of cellular compartments like dendrites and somas. Scale bars 50 μm, respectively.

Subsequently, the leaf has been replaced by a thin brain slice of a transgenic Thy1-GFP-M mouse which expressed enhanced green fluorescent protein (eGFP) in a sparse subset of neuronal populations. For a long-time stability the slice has been soaked in Dako fluorescence mounting medium and covered with a 170 μm thick N-BK7 coverslip. Similar to the preceding experimental setup, the endomicroscope has been attached to a five axis stage and moved mechanically in lateral and axial direction to precisely shift the imaged field of view. Moreover, a drop of water between the specimen and the tip of the device avoided spherical aberrations. The subcellular

Biomedical Optics EXPRESS

optical resolution of the probe enabled the visualization of single dendrites and clear distinction of somas up to the edge of the field of view in real time as depicted in Fig. 6. A minor local contrast enhancement has been applied which slightly improved the image quality (see Visualization 1 for video).

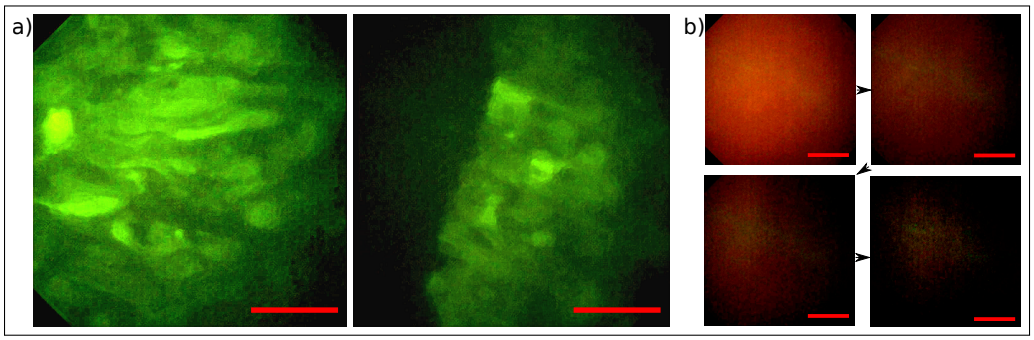

Fig. 7. Image captured with the endomicroscopic probe in epi-direction a) of a cryosection of 10 μm thickness of an experimental tumor expressing eGFP that was grown in an incubated chicken egg. Morphology of tumor tissue could be visualized (left). Healthy tissue (dark) could be accurately distinguished from malignant lesions (bright) at the boundary of the tumor (right). b) Investigation of a glioblastoma biopsy (volume tissue) surgically removed from the brain of a human. Stained in-vivo with 5-Ala. Four adjacent images 150±20 μm apart from each other (top left to bottom right) demonstrate a diffuse delineation capability of the device between malignant (top left), a transition area and healthy tissue (bottom right). Scale bars 50 μm, respectively.

With respect of another potential application, we imaged tumor tissue and aimed for a differentiation from adjacent healthy regions on a cellular level. Therefore, a thin section of an experimental tumor derived from the glioma cell line U87 expressing eGFP that was grown on the chorioallantoic membrane of an incubated chicken egg has been imaged with the endomicroscopic probe. Figure 7(a) and Fig. 7(b) depict the resulting images showing the morphology of the malignant lesions as well as a clear distinction from adjacent healthy tissue (dark). Thereafter, we imaged bulk tissue samples of a fresh glioblastoma biopsy of a patient that received preoperative δ-Aminolevulinic acid (5-Ala) to prove for a potential use in the clinical environment. 5-Ala accumulates in glioblastoma and is metabolized to fluorescent Protoporphyrin IX which therefore allows tumor recognition. The patient gave written consent and the study was approved by the ethics committee at Dresden University Hospital (EK 323122008). Similar to the preceding experiment, the bulk tissue has been covered with a coverslip and the endomicroscope shifted mechanically by a five-axis stage to select the region of interest. Sliding the imaging probe from malignant, red fluorescent tissue towards the healthy region showed a significant drop of intensity as illustrated in Fig. 7(b). The figure illustrates four adjacent view-frames 150±20 μm apart from each other (top left to bottom right) and showcases the potential of the endomicroscopic probe to delineate stained cancer tissue from adjacent regions on a micrometer level in real time. Moreover, a spectral shift of the illumination wavelength towards higher frequencies and thus towards the absorption maximum of 5-Ala will certainly increase the signal in future setups and might allow for a better contrast in upcoming experiments.

Subsequently, a thin tissue section of an unstained human hippocampus resected during an autopsy (anonymous body donation) has been placed in front of the endomicroscope and imaged in epi-direction by collecting the autofluorescence signal. The tissue constituted of different cell layers that could be unambiguously discerned by visual inspection. In Fig. 8(a) we could image the contours of pyramidal cells. The autofluorescent structures matched in size, shape

Biomedical Optics EXPRESS

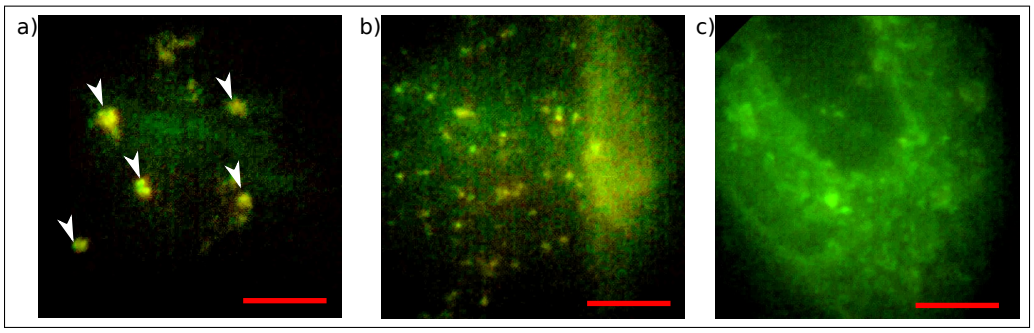

Fig. 8. Images captured with the endomicroscope in epi-direction. a) Contours of pyramidal cells (white arrows) and b) Lipofuscin (granular depositions) visualized in autofluorescence mode in a thin unstained section of a human hippocampus. c) Autofluorescence signal of a thin section of unstained human brain tissue illustrates the transverse section of a blood vessel. Scale bars 50 μm, respectively.

and position pyramidal cells that were shown to exhibit strong endogenous fluorescence of lipofuscin in recent publications [36, 45]. Moreover, a significant response has been detected from numerous granular depositions of Lipofuscin as depicted in Fig. 8(b) which accumulates in the brain during aging. The broad emission spectrum leads to significant signals in the red and green channel of the image and is thus an indicator for lipofuscin [36, 46, 48]. Subsequently, we visualized the transverse section of a blood vessel and clearly distinguished the tissue from adjacent regions in autofluorescence mode as depicted in Fig. 8(c). Large blood vessels can be assessed by fluorescence of elastin fibers as reviewed in [47].

2.4. *In-vivo brain imaging in transgenic Thy1-GFP-M mice*

All animal experiments were performed under the German animal welfare guidelines and have been approved under the no. 55.2-1-54-2532.0-29-14. Thanks to the minimal spatial extent of the probe, a significantly reduced weight compared to state-of-the-art objectives, an easy plug-and-play capability and a simultaneous sub-micrometer resolution within a large field of view, the presented probe can gather a pronounced interest for future experiments in the neuroscience community when imaging neuronal cells in freely moving animals. To indicate the potential for a use in the neuroscience community we placed an anesthetized transgenic Thy1-GFP-M mouse underneath the endomicroscopic probe. A small bone flap of the skull of the rodent has been replaced by a 170 μm thick cranial window made of N-BK7 which was permanently sealed in place providing a clear vision on the somatosensory cortex. The use of a cranial window presents a widespread technique in the neuroscience community for long-term studies in living rodents when imaging the same brain area over months with arbitrary time intervals [50, 51]. Therefore, we anesthetized the mammal by injection of ketamine/xylazine (140/10 mg/kg body weight; WDT/Bayer Health Care) and placed it on a heated stage shown in the background of Fig. 9(a). Furthermore, the probe has been fixed to a five-axis stage which is seen in the front of the picture to precisely control the lateral and axial position as well as the tilt of the probe with respect to the rodent head. Similar to the foregoing ex-vivo experiments, a small drop of water prevented an air gap between the cranial window implemented in the head of the rodent and the front window of the probe. The obtained images are illustrated in Fig. 9(b) and Fig. 9(c) and result from living tissue up to 60 μm deep.

Therewith, we could image small cerebral blood vessels and dendritic cells [49] as depicted in Fig. 9(b). Besides, we could clearly visualize single apical dendrites through a cranial window

Biomedical Optics EXPRESS

embedded in the skull of living, anesthetized animals as demonstrated in Fig. 9(c). Those dendrites arise from cell bodies located in deeper cortical layers of the neocortex which are not visible at depths of up to 60 μm.

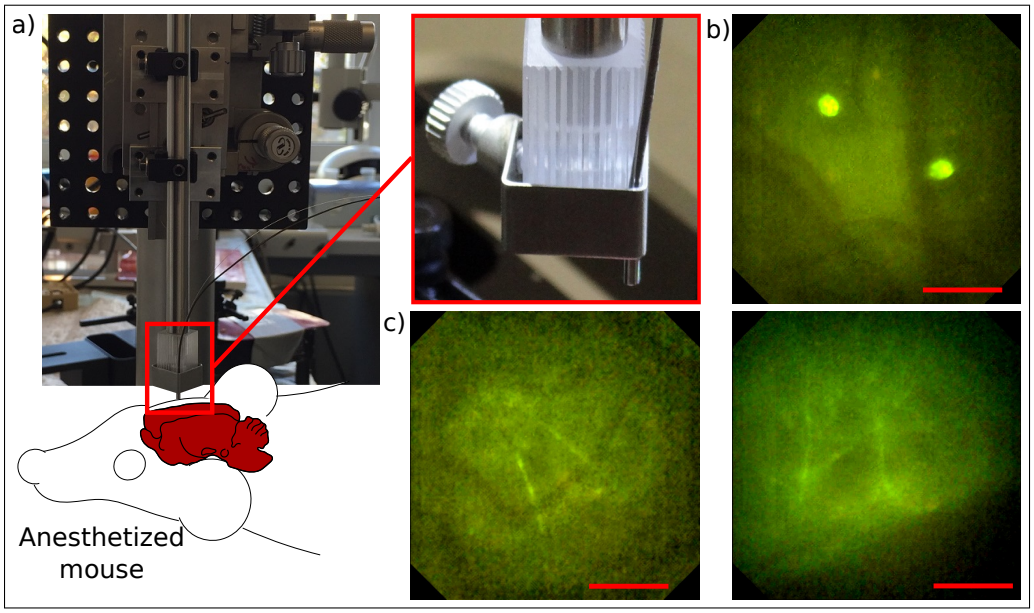

Fig. 9. In-vivo imaging of neuronal cells through a cranial window implanted in the skull of an anesthetized Thy1-GFP-M mouse expressing green fluorescent protein in a sparse subset of neurons. a) Mouse has been placed on a heated stage. The endomicroscopic probe has been moved precisely by a five-axis-stage in lateral and axial direction to sharply image the region of interest. b) Visualization of dendritic cells and blood vessels directly below the cranial window. c) Measurements at up to 60 μm deep inside layer I of the neocortex reveals single dendrites and blood vessels. Scale bars 50 μm, respectively.

2.5. *In-vivo human application*

The final step towards a medical application is to prove the in-vivo imaging ability of the device in humans. Within a self experiment we had the chance to demonstrate in simplified setups that the probe can prospectively support physicians in diagnostic investigations or surgical interventions. Therefore, we assembled a probe with a slightly different working distance of 60 μm in tissue without the requirement of using a 170 μm thick N-BK7 cover window as a coverslip. The design as well as experiments with the assembly didn't lead to a significant change in optical performance. To improve the handling properties for the prove of principle experiment we put the probe into a provisional movable metal arm. The metal sleeve is depicted in Fig. 10(a) and has a rigid length (1) of 14.5 cm with a diameter of 2.3 mm and an additional movable part (2) with a length of 47.5 cm and a diameter of 5.0 mm. We considerably downgraded the flexibility and tininess of the probe with the robust mounting but simultaneously opened up access to the medical environment at the current stage of development.

In a first trial, we locally stained the inner part of the mouth of a human by applying a drop of 10-percent fluorescein, which represents one of the few non-toxic and medically licensed fluorescent dyes for this spectral regime. As depicted in Fig. 10(b), we imaged the contours of single blood cells and could even visualize the peristaltic transport of blood cells in

Biomedical Optics EXPRESS

micro-blood-vessels in real time (see Visualization 2). Finally, we intravenously injected 1 ml of 10-percent fluorescein (ALCON) into the volunteer's arm and therewith achieved an imaging capability of single cells in the mouth of a human. Unfortunately, the contrast is rather poor and the contours of the cells could be localized hardly. The reason for the poor imaging capability might be a missing confocality of the setup but also simply a working distance which was too large for this application. Hence, future setups for medical applications aim at the decrease of the working distance to lie in between 0 μm and 50 μm which has been approved to work in similar but confocally aligned experiments in medical fields [16, 19].

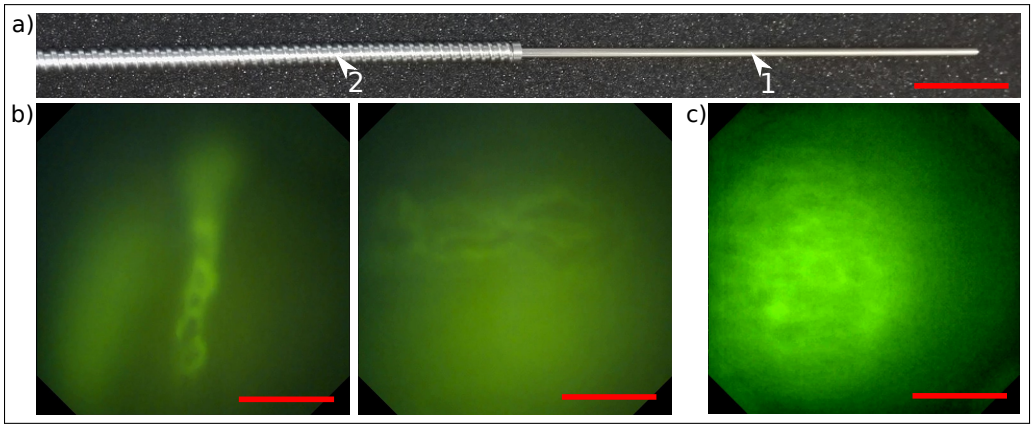

Fig. 10. a) The endomicroscope has been assembled into a provisional metal sleeve with a rigid length/diameter of 14.5 cm / 2.3 mm (1) and an additional movable part with a length/diameter of 47.5 cm / 5.0 mm (2) to improve the handling properties of the probe in the medical environment. Scale bar 3 cm. b) Cell flow in blood vessels can be imaged in real time in the mouth of a human by locally staining the area under observation with fluorescein (ALCON). c) By intraveneous injection of 1 ml 10-percent fluorescein into the volunteer's arm we could detect the contours of single cells after a slight post-processing local contrast enhancement. Scale bars b) and c) 50 μm, respectively.

3. Summary

In conclusion, we demonstrate a stand alone, versatile applicable, very flexible one-photon-epifluorescence endomicroscope which enables for less invasive in-vivo probing of biological tissue. A significant miniaturization of state-of-the-art microscope setups is realized by a double deflection approach integrated in the tiny rigid tip of the endomicroscope by incorporating a side-fire fiber and a dichroic long-pass filter. To further miniaturize the device, simplify the optical setup and improve the flexibility significantly we implemented a miniaturized CMOS image sensor with more than 150,000 pixels at the proximal side of the rigid part which captures the resulting image in RGB channels and real time with 30 fps. The 60 mg light rigid tip with a diameter of 1.6 mm and a length of 6.7 mm is connected with two highly flexible cables and allows, thanks to its filigree nature, the visualization of hardly accessible regions which are far too deep inside the body or the organ to reach with conventional table top microscopes. A quadratic field of view with a side length of more than 160 μm is imaged with a numerical aperture of 0.7 which allows a submicrometer resolution and hence the observation of subcellular structures, assures for a bright and high-contrast image and enables the user to keep an overview during the intervention. Fluorescence edge response function measurements revealed a resolution of 0.74±0.08 μm independently of the field point position. Subsequently, we tested the device by

Biomedical Optics EXPRESS

imaging biological probes ex-vivo and showed a large potential for further research and treatment applications in medical and biomedical fields. Finally, we investigated the imaging performance in-vivo by imaging single dendrites in the layer I of the neocortex of an anesthetized Thy1-GFP-M mouse and captured the cell-flow in the mouth of a human by locally staining the area of interest with fluorescein. Moreover, slight contours of cells in the mouth of a human could be displayed by an intravenous injection of fluorescein. Furthermore, we see a large potential of the device to image neuronal cells in-vivo in freely moving rodents over long time periods. However, due to a strict time schedule and a missing opportunity we abstained from such experiments in the current state of development.

The experiments performed with the presented endomicroscopic probe exposed an excellent optical performance which can even compete with what has been achieved by table-top microscopes. However, necessary improvements have been revealed during the experiments to better adapt the device to the particular application. This means, that neuroscience applications like Ca^{2+} imaging experiments usually require a greater working distance and a larger field of view while accepting a reduced resolution on a cellular rather than on a sub-cellular level. On the contrary, probes which are aimed for future medical applications require the realized subcellular resolution but may improve their imaging performance by further decreasing the working distance. The handling of possible tissue motion artifacts will need to be part of future investigations. The current state of development, however, clearly motivates further investigations and indicates a broad scope of application in the near future.

Funding

This study was supported by the German Ministry of Education and Research (BMBF, project Screen4Tau, grant 13N127-74/75/77/78) and we would like to thank Hans-Joachim Schwarzmaier for project guidance.

Acknowledgments

The authors would like to thank Thomas Raack and his steady hands during the assembly process as well as all other coworkers of GRINTECH GmbH and the entire project consortium for their reliable work. Moreover, a special thanks goes to Dr. Anna Englhardt, Dr. Veronika Volgger and Dr. Roberta Galli for their engagement in the experiments.

Disclosures

P: W.G. and B.M. are authors on a patent application for the layout of the endomicroscopic system (US2016235278A1).
E: G.M., B.M., M.K. and S.F. are full-time employees of Grintech GmbH. W.G., A.E. and K.-M.I. are full-time employees of Karl Storz GmbH & Co. KG.